

Improving Effectiveness of the Double Layer Method for Modeling of Three-Dimensional Magnetic Field of Electromagnetic Systems

Dmitriy M. Filippov^{1, *}, Alexandr A. Shuyskiy¹, Gennadiy P. Kozik¹,
Dmitry V. Samokhvalov², and Anatoliy N. Kazak¹

Abstract—When solving the boundary integral equation with respect to the density of a double layer of fictitious magnetic charges in the case of using a piecewise constant approximation of double layer density, the interface conditions for the field vectors are not fulfilled at any point of the interface between ferromagnetic media. The article shows that these interface conditions are satisfied not discretely but integrally. Based on the proposed integral relations, which are derived from the Ampere’s Circuital Law, a new system of linear equations is derived. The system of linear equations is obtained with respect to the piecewise constant approximation coefficients of double layer magnetic charge density. The resulting system of equations does not contain the scalar magnetic potential of free sources. Consequently, this numerical model can be directly applied to the analysis of magnetic field in any multiply connected domains without introducing impenetrable partitions or solving an additional boundary value problem for finding scalar magnetic potential.

1. INTRODUCTION

The method of integral equations is known in the scientific literature as boundary element method (BEM) [1–3]. There are two different widespread formulations of BEM: “Direct boundary element method formulation” and “Indirect boundary element method formulation” [4].

The direct formulation of BEM is based on the direct application of Green’s theorem to obtain the integral equation [4]. The indirect formulation is based on solving boundary integral equations for the densities of secondary sources (surface charge densities) [4]. In this article, the indirect formulation is called the secondary sources method, since such a name reflects the physical meaning of this method. Surface secondary sources can be: a single layer of charges [5–7], a double layer of charges [8–13], a single layer of currents [14], and a double layer of currents [13]. Some of the types of secondary sources are equivalent to real field sources that can be observed experimentally. For example, such real secondary sources include a single layer of electric charges, a double layer of electric charges (or a layer of electric dipoles), a single layer of magnetization currents (or a layer of microcurrents), and a double layer of currents (or a layer of magnetic moments). Some types of secondary sources have no natural equivalents and are mathematical abstractions. Such secondary sources are usually called fictitious ones. These include, for example, a single layer of fictitious magnetic charges and a double layer of fictitious magnetic charges. In addition to surface secondary sources, there are also volume secondary sources, for example, the volume density of eddy currents [15].

All types of secondary sources can be divided into scalar (their distribution is described by scalar functions) and vector (their distribution is described by vector functions). If the problem of calculating the field is formulated in the case of a three-dimensional formulation, and the geometry of

Received 11 November 2020, Accepted 11 December 2020, Scheduled 22 December 2020

* Corresponding author: Dmitriy M. Filippov (filippov.dm@cfuv.ru).

¹ V.I. Vernadsky Crimean Federal University, Simferopol 295007, Russia. ² Saint Petersburg Electrotechnical University “LETI”, Saint Petersburg 197376, Russia.

the computational domain is rather complicated, then one should use scalar secondary sources. Such sources include a single layer of charges and a double layer of charges. Generally speaking, a single layer of charges has some disadvantages compared to a double layer of charges. First, a single layer of charges almost always (it depends on the geometry of the computational domain) is a function containing a finite number of essential discontinuity points in its domain. Usually, this property is the reason for the low computational effectiveness of the calculation method, which is based on the use of a single layer of charges as secondary sources. However, in [15], using a single layer of electric charges as an example, it is shown how this problem can be solved, and the computational effectiveness of the method can be increased. The method proposed in [15] is applicable to a single layer of fictitious magnetic charges. Secondly, when calculating the electromagnetic field, if it becomes necessary to calculate the vector potential of the magnetic field, a single layer of fictitious charges is of little use. This is because calculating the vector potential as a function of density of a magnetic charge single layer turns into an unnecessarily difficult mathematical problem. At the same time, there is a simple expression for the vector potential created by a double layer of fictitious magnetic charges. In addition, the surface density of the double layer of charges (both electric and magnetic) never has essential discontinuity points, no matter how complex the geometry of the computational domain is.

The above reasoning is a convincing argument in favor of choosing a method based on the use of a double layer of fictitious magnetic charges as a method for calculating the three-dimensional magnetic field of electromagnetic systems. Consider this method in more details.

2. CLASSICAL INTEGRAL EQUATION WITH RESPECT TO A DOUBLE LAYER OF MAGNETIC CHARGES

2.1. Features of the Integral Equation with Respect to a Double Layer of Magnetic Charges

In [11], the integral equation for the density of a double layer of magnetic charges is obtained. This equation is derived from the interface condition for the magnetic field vector taking into account the continuity property of the double layer potential. We represent this equation in the following form:

$$\nu(Q) + \frac{\lambda}{2\pi} \oint_S \nu(P) \frac{(\mathbf{n}_P, \mathbf{r}_{PQ})}{r_{PQ}^3} dS_P = -2\lambda\varphi_0(Q) + C, \quad (1)$$

where $\nu(Q)$ is the density of the double layer at points $Q \in S$; S is the boundary of the region occupied by a ferromagnetic with magnetic permeability μ ; $\lambda = (\mu - \mu_0)/(\mu + \mu_0)$; \mathbf{n}_P is the external normal to the point $P \in S$; \mathbf{r}_{PQ} is a radius-vector drawn from point $P \in S$ to point $Q \in S$; $\varphi_0(Q)$ is the scalar magnetic potential of the primary field sources at a point $Q \in S$; C is a constant.

The scalar magnetic potential is introduced by the expression:

$$\mathbf{B} = -\mathbf{grad}\varphi, \quad (2)$$

where \mathbf{B} is the magnetic flux density.

After solving Equation (1) regarding the density of the double layer $\nu(Q)$ a magnetic field can be calculated at any point in space created by primary and secondary sources according to the following expression:

$$\mathbf{B}(M) = \frac{1}{4\pi} \oint_S \nu(P) \frac{3(\mathbf{r}_{PQ}, \mathbf{n}_P) \mathbf{r}_{PQ} - r_{PQ}^2 \mathbf{n}_P}{r_{PQ}^5} dS_P + \mathbf{B}_0(M), \quad (3)$$

where M is an arbitrary point in space; $\mathbf{B}_0(M)$ is the magnetic flux density of the primary field sources.

Equation (1) has one significant drawback: on the right-hand side they contain a scalar magnetic potential. In a multiply connected area, this function is not single-valued. For the correct calculation of the magnetic scalar potential, it is necessary to introduce conditional impermeable partitions. We show this with a simple example (Figure 1).

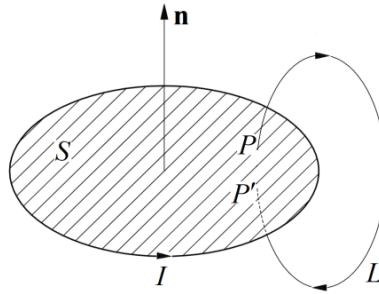


Figure 1. Current coil and impermeable partition.

The points P and P' are infinitely close to each other; therefore, the integration path L differs infinitely little from a closed loop $PP'P$. Therefore, we can write the following ratio:

$$\varphi_0(P) - \varphi_0(P') = \oint_{PP'P} \mathbf{B}_0 d\mathbf{l} = \mu_0 I, \tag{4}$$

where \mathbf{B}_0 is the magnetic flux density of free sources.

It can be seen from the considered example that the result of calculating the scalar magnetic potential depends on the integration path. To avoid using a multi-valued function, conditional impermeable partitions are introduced (in Figure 1, such a partition is shown by hatching). Then it is possible to carry out integration over any circuit if it does not cross the partition. This technique allows you to get simply connected from a multiply connected area.

The procedure for introducing conditional impermeable partitions is very difficult to automate. In some problems, when the computational domain contains many current loops, the planes of which can overlap, the task of introducing conditional partitions can be unacceptably time-consuming.

In this regard, in the present work, it is proposed to modify the double layer method of magnetic charges. Namely, new equations are proposed. The solution of these equations does not require the calculation of a scalar magnetic potential.

2.2. Fulfillment of the Interface Conditions for a Piecewise Constant Approximation of Density of a Magnetic Charge Double Layer

Integral Equation (1) is derived from the following interface condition:

$$\varphi(Q^+)/\mu = \varphi(Q^-)/\mu_0, \tag{5}$$

where φ is the scalar magnetic potential created by primary and secondary field sources; Q^+ is the boundary limit point inside the region with magnetic permeability μ ; Q^- is the boundary limit point inside the region with magnetic permeability μ_0 (Figure 2).

Consider a piecewise constant approximation of the density of a magnetic charge double layer. To do this, we divide, in some way, the surface S of a ferromagnetic into N elements. Within the limits of each such element of the partition, we impose the condition that $\nu(Q) = \nu_k = \text{const}$ ($k = 1, 2, \dots, N$).

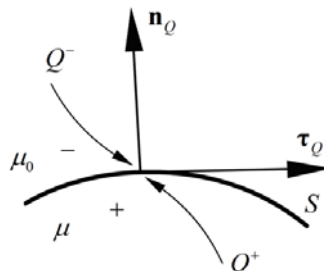


Figure 2. The boundary between the regions filled with ferromagnetic and air.

Introduce a vector $\boldsymbol{\tau}_Q$ at a point Q , which is tangential to the surface (and is orthogonal to a normal vector \mathbf{n}_Q in Figure 2). Then, under the condition of a piecewise constant approximation of the double layer density, it is easy to obtain the equality:

$$\partial\varphi(Q^+)/\partial\tau = \partial\varphi(Q^-)/\partial\tau.$$

But then it is obvious:

$$(1/\mu)\partial\varphi(Q^+)/\partial\tau \neq (1/\mu_0)\partial\varphi(Q^-)/\partial\tau. \quad (6)$$

From Eq. (6) the inequality follows:

$$(\mathbf{H}(Q^+), \boldsymbol{\tau}_Q) \neq (\mathbf{H}(Q^-), \boldsymbol{\tau}_Q)$$

(the expression in brackets means the dot product of the magnetic field strength vector by the vector tangent to the boundary at the observation point). In other words, the interface condition for the vector of the magnetic field strength is not fulfilled at any point of the boundary in the case of a piecewise constant approximation of double layer density.

Show that when using a piecewise constant approximation of double layer density, the interface condition for the vector of magnetic field strength is fulfilled integrally.

Since the integral Equation (1) is derived from the interface condition in Eq. (5), in the case of a piecewise constant approximation of the double layer density, the following equations must be fulfilled:

$$\begin{aligned} \varphi(Q_1^+)/\mu &= \varphi(Q_1^-)/\mu_0, \quad \varphi(Q_2^+)/\mu = \varphi(Q_2^-)/\mu_0, \quad \dots, \\ \varphi(Q_k^+)/\mu &= \varphi(Q_k^-)/\mu_0, \quad \dots, \quad \varphi(Q_N^+)/\mu = \varphi(Q_N^-)/\mu_0. \end{aligned} \quad (7)$$

From Eq. (7) the following equalities follow:

$$[\varphi(Q_{k+1}^+) - \varphi(Q_k^+)]/\mu = [\varphi(Q_{k+1}^-) - \varphi(Q_k^-)]/\mu_0, \quad k = 1, 2, \dots, N. \quad (8)$$

Taking into account Eqs. (2) and (8), we obtain:

$$\frac{1}{\mu} \int_{Q_k^+}^{Q_{k+1}^+} \mathbf{B}^+ \boldsymbol{\tau}_Q dl = \frac{1}{\mu_0} \int_{Q_k^-}^{Q_{k+1}^-} \mathbf{B}^- \boldsymbol{\tau}_Q dl, \quad k = 1, 2, \dots, N$$

or

$$\int_{Q_k^+}^{Q_{k+1}^+} \mathbf{H}^+ \boldsymbol{\tau}_Q dl = \int_{Q_k^-}^{Q_{k+1}^-} \mathbf{H}^- \boldsymbol{\tau}_Q dl, \quad k = 1, 2, \dots, N. \quad (9)$$

Expression (9) is the law Ampere's Circuital Law in integral form for a path that is infinitely close to a boundary and passes through the points Q_k and Q_{k+1} . These points lie inside any two neighboring elements of the mesh. These points can, for example, be located at the geometric centers of the specified elements.

Show that expressions (9) can be used as interface conditions for obtaining new equations with respect to the density of a magnetic charge double layer. Moreover, these equations are free of the disadvantages that are inherent in Equation (1).

3. NEW EQUATIONS FOR THE METHOD OF MAGNETIC CHARGE DOUBLE LAYER

Consider a ferromagnetic sample with its volume V that is covered by surface S and is filled with substance which has magnetic permeability μ . A ferromagnetic sample is placed in an external magnetic field of free sources $\mathbf{B}_0(x, y, z)$. Impose that a surface of a ferromagnetic sample is meshed into N triangular elements (Figure 3).

Figure 3 shows a triangular element of a mesh containing a point Q_k (we call it the k -th element). This element is surrounded by three more triangles, the numbers of which are i_1 , i_2 and i_3 . On the right in Figure 3, a fragment of the sample surface is shown on an enlarged scale. A closed contour is drawn

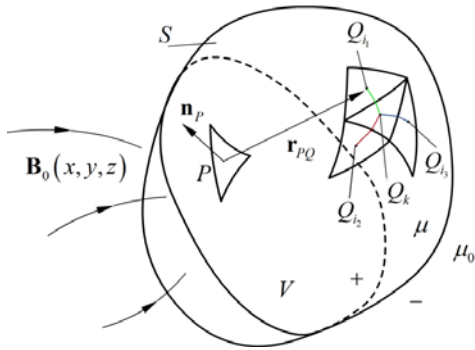


Figure 3. Ferromagnetic sample in an external magnetic field.

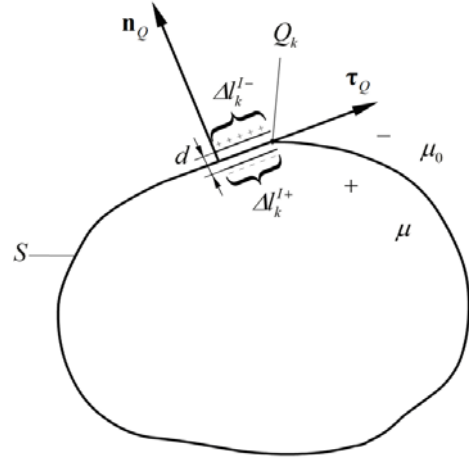


Figure 4. Section of a ferromagnetic sample along a segment Δl_k^I .

through points Q_k and Q_{i1} . A part of this contour is located in the “-” area, and a part is located in the “+” area (Figure 3). Draw, for example, along the segment Δl_k^I , indicated in Figure 3, section of a ferromagnetic sample (Figure 4).

Figure 4 shows a fragment of a double layer located within the k -th element of a mesh. It is presented in the form of two oppositely charged single layers, which are located symmetrically relative to the boundary at a small distance d from each other.

An open path consists of three lines: Δl_k^{I+} , d , and Δl_k^{I-} . An open contour that covers the element of a mesh i_1 is constructed in a similar way. Contours $\Delta l_k^{I+} \cup d \cup \Delta l_k^{I-}$ and $\Delta l_k^{II-} \cup d \cup \Delta l_k^{II+}$ are connected at the border between elements and form a closed contour $\Delta l_k^{II+} \cup \Delta l_k^{I+} \cup d \cup \Delta l_k^{I-} \cup \Delta l_k^{II-} \cup d$.

Present the derivation of new equations for a double layer of magnetic charges.

3.1. Derivation of a New System of Equations for a Piecewise Constant Approximation of the Density of a Magnetic Charge Double Layer

Write down the Ampere’s Circuital Law in integral form for the path passing through the points Q_k and Q_{i1} similar to expression (9). Using the denotations in Figure 3 and Figure 4, we obtain:

$$\int_{\Delta l_k^{II+}} \mathbf{H}^+ \boldsymbol{\tau}_Q dl_Q + \int_{\Delta l_k^{I+}} \mathbf{H}^+ \boldsymbol{\tau}_Q dl_Q = \int_{\Delta l_k^{II-}} \mathbf{H}^- \boldsymbol{\tau}_Q dl_Q + \int_{\Delta l_{k+1}^{II-}} \mathbf{H}^- \boldsymbol{\tau}_Q dl_Q. \quad (10)$$

Equation (10) can be rewritten as follows:

$$\begin{aligned} & \frac{1}{\mu} \int_{\Delta l_k^{II+}} (\mathbf{B}_0 + \mathbf{B}_\nu + \mathbf{B}_{\nu Q}^+) \boldsymbol{\tau}_Q dl_Q + \frac{1}{\mu} \int_{\Delta l_k^{I+}} (\mathbf{B}_0 + \mathbf{B}_\nu + \mathbf{B}_{\nu Q}^+) \boldsymbol{\tau}_Q dl_Q \\ &= \frac{1}{\mu_0} \int_{\Delta l_k^{II-}} (\mathbf{B}_0 + \mathbf{B}_\nu + \mathbf{B}_{\nu Q}^-) \boldsymbol{\tau}_Q dl_Q + \frac{1}{\mu_0} \int_{\Delta l_k^{II-}} (\mathbf{B}_0 + \mathbf{B}_\nu + \mathbf{B}_{\nu Q}^-) \boldsymbol{\tau}_Q dl_Q. \end{aligned} \quad (11)$$

where \mathbf{B}_0 is the magnetic flux density of free sources (Figure 3); $\mathbf{B}_{\nu Q}$ is the magnetic flux density at points of the integration contour due to the double layer of the mesh element that is covered by this integration contour; \mathbf{B}_ν is the magnetic flux density due to the double layer of magnetic charges of all other elements of a mesh.

It is obvious that

$$\int_{\Delta l_k^{II+}} \mathbf{B}_0 \tau_Q dl_Q + \int_{\Delta l_k^{I+}} \mathbf{B}_0 \tau_Q dl_Q = \int_{\Delta l_k^{I-}} \mathbf{B}_0 \tau_Q dl_Q + \int_{\Delta l_k^{II-}} \mathbf{B}_0 \tau_Q dl_Q, \quad (12)$$

$$\int_{\Delta l_k^{II+}} \mathbf{B}_\nu \tau_Q dl_Q + \int_{\Delta l_k^{I+}} \mathbf{B}_\nu \tau_Q dl_Q = \int_{\Delta l_k^{I-}} \mathbf{B}_\nu \tau_Q dl_Q + \int_{\Delta l_k^{II-}} \mathbf{B}_\nu \tau_Q dl_Q. \quad (13)$$

We denote the integrals in Eqs. (12) and (13), respectively:

$$\int_{\Delta l_k^{II} + \Delta l_k^I} \mathbf{B}_0 \tau_Q dl_Q \quad \text{and} \quad \int_{\Delta l_k^{II} + \Delta l_k^I} \mathbf{B}_\nu \tau_Q dl_Q.$$

Taking this into account, expression (11) takes the form:

$$\begin{aligned} & \left(\frac{1}{\mu} - \frac{1}{\mu_0} \right) \int_{\Delta l_k^{II} + \Delta l_k^I} \mathbf{B}_0 \tau_Q dl_Q + \left(\frac{1}{\mu} - \frac{1}{\mu_0} \right) \int_{\Delta l_k^{II} + \Delta l_k^I} \mathbf{B}_\nu \tau_Q dl_Q \\ & + \frac{1}{\mu} \int_{\Delta l_k^{II+} + \Delta l_k^{I+}} \mathbf{B}_{\nu_Q}^+ \tau_Q dl_Q - \frac{1}{\mu_0} \int_{\Delta l_k^{I-} + \Delta l_k^{II-}} \mathbf{B}_{\nu_Q}^- \tau_Q dl_Q = 0. \end{aligned} \quad (14)$$

Take into account that a double layer of magnetic charges is two oppositely charged single layers located close to each other. The distance between the layers is indicated by d . This is illustrated in Figure 4. The figure shows a layer of positive charges and a layer of negative charges in a certain local area of a surface. We denote the density of a single layer by σ . Then the relation between the double and a single layer of magnetic charges is given by the following expression: $\nu = \sigma d$.

Then, in accordance with the Ampere's Circuital Law for a vector \mathbf{B} , we can write the expression:

$$\int_{\Delta l_k^{II+} + \Delta l_k^{I+}} \mathbf{B}_{\nu_Q}^+ \tau_Q dl_Q - \int_{\Delta l_k^{I-} + \Delta l_k^{II-}} \mathbf{B}_{\nu_Q}^- \tau_Q dl_Q - \nu_k + \nu_{i_1} = 0. \quad (15)$$

Symmetry implies:

$$- \int_{\Delta l_k^{I-} + \Delta l_k^{II-}} \mathbf{B}_{\nu_Q}^- \tau_Q dl_Q = \int_{\Delta l_k^{II+} + \Delta l_k^{I+}} \mathbf{B}_{\nu_Q}^+ \tau_Q dl_Q.$$

Therefore, from Eq. (15) the expression follows:

$$\int_{\Delta l_k^{II} + \Delta l_k^I} \mathbf{B}_{\nu_Q} \tau_Q dl_Q = \frac{\nu_k}{2} - \frac{\nu_{i_1}}{2}. \quad (16)$$

Finally, consider the integral in Eq. (14) which contains the function $\mathbf{B}_\nu \tau_Q$. We represent this integral as a sum of integrals:

$$\begin{aligned} \int_{\Delta l_k^{II} + \Delta l_k^I} \mathbf{B}_\nu \tau_Q dl_Q &= \sum_{\substack{m=1 \\ m \neq k}}^N \nu_m \int_{\Delta l_k^I} \tau_Q \int_{\Delta S_m} \frac{3(\mathbf{r}_{PQ}, \mathbf{n}_P) \mathbf{r}_{PQ} - r_{pQ}^2 \mathbf{n}_P}{r_{pQ}^5} dS_P dl_Q \\ &+ \sum_{\substack{m=1 \\ m \neq i_2}}^N \nu_m \int_{\Delta l_k^{II}} \tau_Q \int_{\Delta S_m} \frac{3(\mathbf{r}_{PQ}, \mathbf{n}_P) \mathbf{r}_{PQ} - r_{pQ}^2 \mathbf{n}_P}{r_{pQ}^5} dS_P dl_Q. \end{aligned} \quad (17)$$

Here, expression (3) is applied, namely the term for calculating the magnetic flux density, which is created by a double layer of magnetic charges.

If we substitute Eqs. (17) and (16) into Eq. (14), then we get the equation written for a closed loop passing through the points Q_k and Q_{i_1} . However, we write this equation in a generalized form (for this we introduce new superscripts and a subscript). Then we get the required system of equations:

$$\begin{aligned} & \nu_i - \nu_k - \frac{\lambda}{2\pi} \left\{ \sum_{\substack{m=1 \\ m \neq k}}^N \nu_m \int_{\Delta l_k^J} \tau_Q \int_{\Delta S_m} \mathbf{K}(P, Q) dS_P dl_Q + \sum_{\substack{m=1 \\ m \neq i}}^N \nu_m \int_{\Delta l_k^U} \tau_Q \int_{\Delta S_m} \mathbf{K}(P, Q) dS_P dl_Q \right\} \\ & = 2\lambda \int_{\Delta l_k^J + \Delta l_k^U} \mathbf{B}_0 \tau_Q dl_Q, \end{aligned} \quad (18)$$

where $\mathbf{K}(P, Q) = [3(\mathbf{r}_{PQ}, \mathbf{n}_P) \mathbf{r}_{PQ} - r_{PQ}^2 \mathbf{n}_P] / r_{PQ}^5$; $\lambda = (\mu - \mu_0) / (\mu + \mu_0)$; $i = i_1, i_2, i_3$; $J = I, III, V$; $U = II, IV, VI$; $k = 1, 2, \dots, N$.

It is denoted in Eq. (18): i is the subscript of one of the three elements that share a common border with the k -th element; J is the superscript at the segment Δl_k^J , which denotes the number of one of the three segments belonging to the k -th element (only one of these three segments is denoted in Figure 3 (in the fragment on the right), namely Δl_k^I , it is green; segment Δl_k^{III} is red; segment Δl_k^V is blue); U is the superscript at the segment Δl_k^U , which denotes the number of the segment belonging to either the element with the subscript i_1 (segment Δl_k^{II} that is green in Figure 3), or the element with the subscript i_2 (segment Δl_k^{IV} that is red in Figure 3), or the element with the subscript i_3 (segment Δl_k^{VI} that is blue in Figure 3).

The system of equations in accordance with Eq. (18) is composed as follows: for the selected element number k , the numbers of neighboring triangles are determined, which are i_1, i_2, i_3 (for each k these numbers are different, and in general they are not in any sequence). Then the equation for k and $i = i_1, J = I, U = II$ is written (the corresponding intervals of integration are determined). The next line is the equation for k and $i = i_2, J = III, U = IV$ (the corresponding intervals of integration are determined). The next line is the equation for k and $i = i_3, J = V, U = VI$ (the corresponding intervals of integration are determined).

The system of linear Equation (18) is overdetermined and always has a rectangular matrix. Such a system can be reduced by known methods to a system with a square matrix, and its pseudo-solution can be sought.

However, it is much easier and more rational to act in a different way. Namely, after the corresponding three equations of the form (18) are obtained for each k -th element, it is enough to add together their left-hand and right-hand sides. Thus, one equation is obtained for each element of a mesh, and the system of equations has a square matrix. This approach is quite reasonable, since equations of the form (18) follow from the Ampere's Circuital Law, which is fulfilled for each of the three contours connecting the centers of two neighboring elements.

Note that in general an element of a mesh can have more than three neighboring elements, for example, if the elements are not triangular. Alternatively, if the elements are triangular, but a mesh is not adaptive. For these cases, the method is also applicable, and for each element, as many equations of the form (18) are written as it has neighbors. However, in the opinion of the authors, the easiest way is to use an adaptive mesh, for which each element has only three neighboring elements.

Note also that when implementing this method, the authors placed points Q_k in the geometric centers of the triangular elements of a mesh, and the segments of integration, such as Δl_k^I connecting the points Q_k with the midpoints of the corresponding edges of the triangle.

Draw some important conclusions on the properties of the resulting system of Equation (18).

- 1) The system of Equation (18) does not contain the scalar magnetic potential of free sources and, therefore, can be directly applied to the calculation of the magnetic field in any multiply connected domains without introducing impenetrable partitions or solving an additional boundary value problem for finding the scalar magnetic potential.
- 2) The solution to the system of Equation (18) leads to fulfillment of interface conditions in Eq. (9) written in integral form.

Note that an equation that is equivalent to Eq. (18) was obtained in [16] for the case of two-dimensional magnetic field.

3.2. Calculation of Coefficients of the Linear System (18)

Consider the calculation of the following integral included in coefficients of the system of linear Equation (18):

$$K = \int_{\Delta S_m} \int_{\Delta l_k^J} \frac{3(\mathbf{r}_{PQ}, \mathbf{n}_P) \mathbf{r}_{PQ} - r_{PQ}^2 \mathbf{n}_P}{r_{PQ}^5} \tau_Q dl_Q dS_P. \quad (19)$$

Integration area ΔS_m in Eq. (19) is a triangular element on the surface of a ferromagnetic sample. Integration area Δl_k^J is a segment lying on the surface of some k -th triangular element (Figure 3). These triangular elements are specified in the original global coordinate system by the radius vectors of the vertices and vectors of the outer normals. Figure 3 shows several arbitrary triangles located on the surface of a ferromagnetic sample. For concreteness, the triangle with the normal \mathbf{n}_P on it (it is denoted in Figure 3) has the subscript m , and the triangle with the subscript k is shown in the same Figure 3. Also, for concreteness, we suppose that $J = I$, that is, consider the case when $\Delta l_k^J = \Delta l_k^I$ (Figure 3).

Further, the case of Cartesian coordinates is considered.

Figure 5 shows a line segment located at random in the Cartesian coordinate system associated with the triangular element that is numbered m .

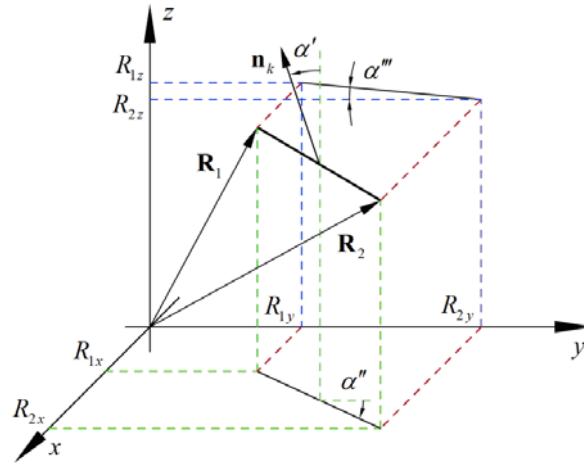


Figure 5. The segment of integration in the Cartesian coordinate system.

Surface integral over the area ΔS_m in Eq. (19) is calculated by numerical methods. To perform this, it is enough to triangulate this area and apply the midpoint rule to calculate the integral. Linear integral on the line Δl_k^I is calculated analytically if you make a transformation to the local coordinate system associated with the k -th triangle.

Denote the normal to the k -th triangle by \mathbf{n}_k (Figure 5). The coordinates of ends of the integration segment are set by radius vectors \mathbf{R}_1 and \mathbf{R}_2 . Present an algorithm that allows transforming an arbitrary vector from a global coordinate system to a local one.

Construct a local coordinate system associated with the k -th triangular element as follows: the unit vector of the Z' -axis matches the unit normal vector \mathbf{n}_k ; the unit vector of the Y' -axis is directed in the same way as the vector $\mathbf{R}_2 - \mathbf{R}_1$; the unit vector of the X' -axis is directed in such a way as to form the right-handed coordinate system $X'Y'Z'$. The origin of the local coordinate system lies in the geometric center of the integration segment Δl_k^I .

Transform coordinates using an arbitrary vector \mathbf{v}_g as an example.

Calculate:

$$\alpha''' = \operatorname{arctg} \left(\frac{R_{1z} - R_{2z}}{R_{2y} - R_{1y}} \right). \quad (20)$$

Further, if the vector \mathbf{v}_g is the radius vector of some point in space, then we carry out a shift along the coordinate axes:

$$\tilde{\mathbf{v}}_g = \mathbf{v}_g - (\mathbf{R}_1 + \mathbf{R}_2)/2. \quad (21)$$

Otherwise, no shift along the coordinate axes is performed (for example, if \mathbf{v}_g is the normal vector, or the difference of two radius vectors), then $\tilde{\mathbf{v}}_g = \mathbf{v}_g$.

Introduce the first rotation matrix:

$$A''' = \begin{pmatrix} 1 & 0 & 0 \\ 0 & \cos \alpha''' & -\sin \alpha''' \\ 0 & \sin \alpha''' & \cos \alpha''' \end{pmatrix}. \quad (22)$$

Next, we multiply the matrix by the vectors:

$$\mathbf{v}_g''' = A''' \tilde{\mathbf{v}}_g; \quad \mathbf{R}_1''' = A''' \mathbf{R}_1; \quad \mathbf{R}_2''' = A''' \mathbf{R}_2; \quad \mathbf{n}_k''' = A''' \mathbf{n}_k.$$

Next, we calculate:

$$\begin{aligned} \alpha'' &= \operatorname{arctg} \left(\frac{R_{2x} - R_{1x}}{R_{2y} - R_{1y}} \right); \\ A'' &= \begin{pmatrix} \cos \alpha'' & -\sin \alpha'' & 0 \\ \sin \alpha'' & \cos \alpha'' & 0 \\ 0 & 0 & 1 \end{pmatrix}; \\ \mathbf{v}_g'' &= A'' \mathbf{v}_g'''; \quad \mathbf{n}_k'' = A'' \mathbf{n}_k'''. \end{aligned} \quad (23)$$

Next, we calculate:

$$\alpha' = \begin{cases} -|\arccos(\mathbf{e}_z, \mathbf{n}_k)|, & \text{if } c_y \leq 0; \\ |\arccos(\mathbf{e}_z, \mathbf{n}_k)|, & \text{if } c_y > 0. \end{cases},$$

where $\mathbf{c} = [\mathbf{e}_z, \mathbf{n}_k]$ is an auxiliary vector needed to determine the rotation of the angle α' ; \mathbf{e}_z is the unit vector along the Z -axis.

We calculate the last rotation matrix and determine the required vector in the local coordinate system:

$$A' = \begin{pmatrix} \cos \alpha' & 0 & -\sin \alpha' \\ 0 & 1 & 0 \\ \sin \alpha' & 0 & \cos \alpha' \end{pmatrix}; \quad (24)$$

$$\mathbf{v}_g' = \mathbf{v}_g. \quad (25)$$

The inverse transformation from the local coordinate system to the global coordinate system is carried out in the same way. To perform this, three rotations must be performed in inverse order changing the signs of all three rotation angles to the opposite ones. It is also necessary to change the sign in the expression of shift along the coordinate axes.

In the local coordinate system, the linear integral included in Eq. (19) takes the following form:

$$K_l(P) = \int_{-L/2}^{L/2} \frac{3 \left(\mathbf{n}'_P, \mathbf{r}'_{PQ} \right) \mathbf{r}'_{PQ} - r'^2_{PQ} \mathbf{n}'_P}{r'^5_{PQ}} \mathbf{e}'_y dy'_Q. \quad (26)$$

Integral in Eq. (26) is calculated analytically using tables of integrals.

4. EXAMPLE OF MODELING AND ANALYSIS OF COMPUTATIONAL EFFICIENCY OF THE METHOD

As an example of application of the developed computational model, consider the modeling of the magnetic field, which is created by the magnetic system of an axial flux electric machine with a coreless stator (Figure 6) [17–19].

The rotor of such a machine consists of two ferromagnetic disks with permanent magnets (Figure 7). The stator is a set of copper coils connected to each other in a three-phase electrical circuit and filled with epoxy compound (Figure 8).

An electric machine with a rated power of 2 kW was manufactured. This machine was tested on the stand (Figure 9).

Figure 10 shows the performance characteristics of the machine, which were obtained on the stand at a rotor speed of 375 rpm (this speed corresponds to a current frequency of 50 Hz).

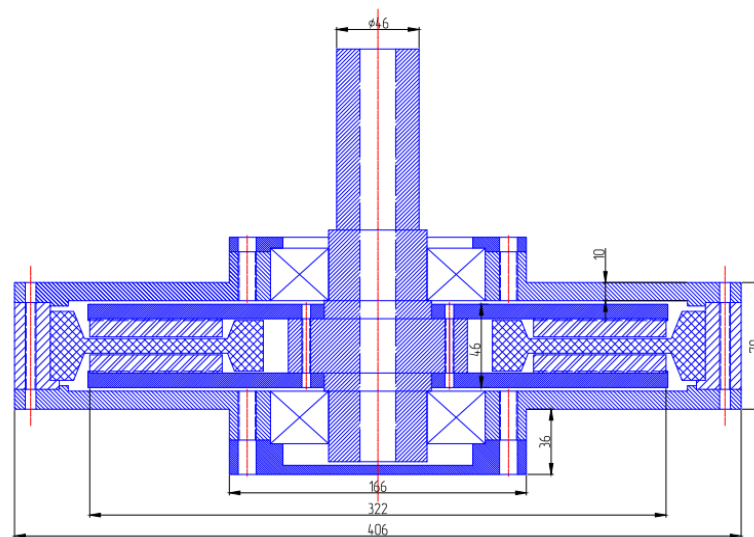


Figure 6. Axial flux electric machine with a coreless stator.



Figure 7. Axial flux machine rotor.

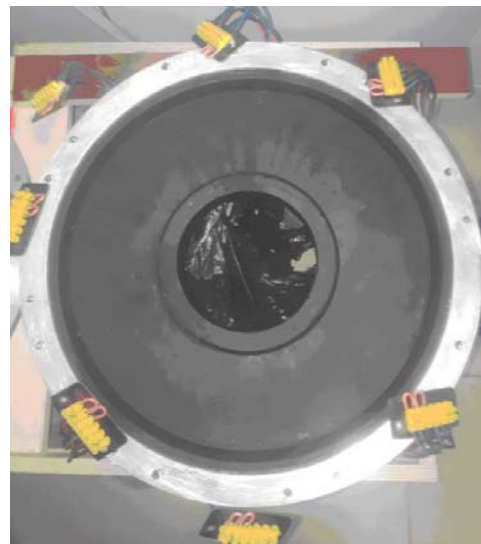


Figure 8. Axial flux machine stator.



Figure 9. The stand for testing electrical machines (from left to right: traction motor; multiplier gearbox, Magtrol TM-311 torque sensor, axial flux machine; a digital multimeter is located on the middle shelf).

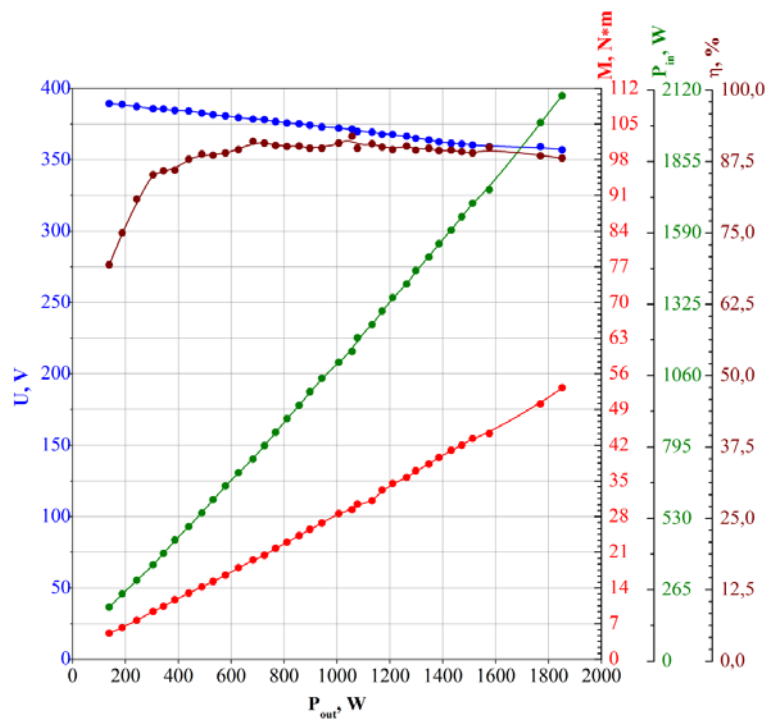


Figure 10. The performance characteristics of the tested electric machine.

Using the developed numerical model in Eq. (18), the magnetic field of the axial flux machine was simulated. Figure 11 shows the triangulation mesh, which was applied when discretizing the surface of disks containing permanent magnets (Figure 7). The total number of triangulation elements for two ferromagnetic disks was 9752. Maximum memory size used in the calculations was 928 Mb. The field of permanent magnets was calculated using a current model according to which each magnet was replaced by a coil with a current $i = Jh$, where J is the magnetization of the permanent magnet, and h is its thickness.

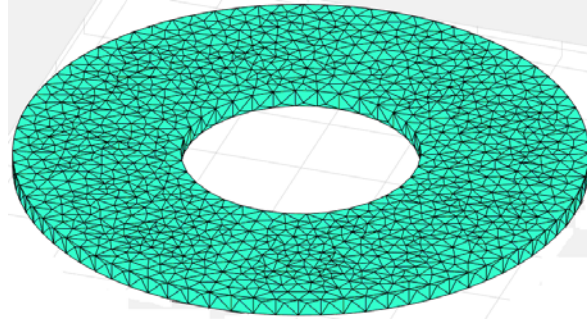


Figure 11. Triangulation of the disk surface.

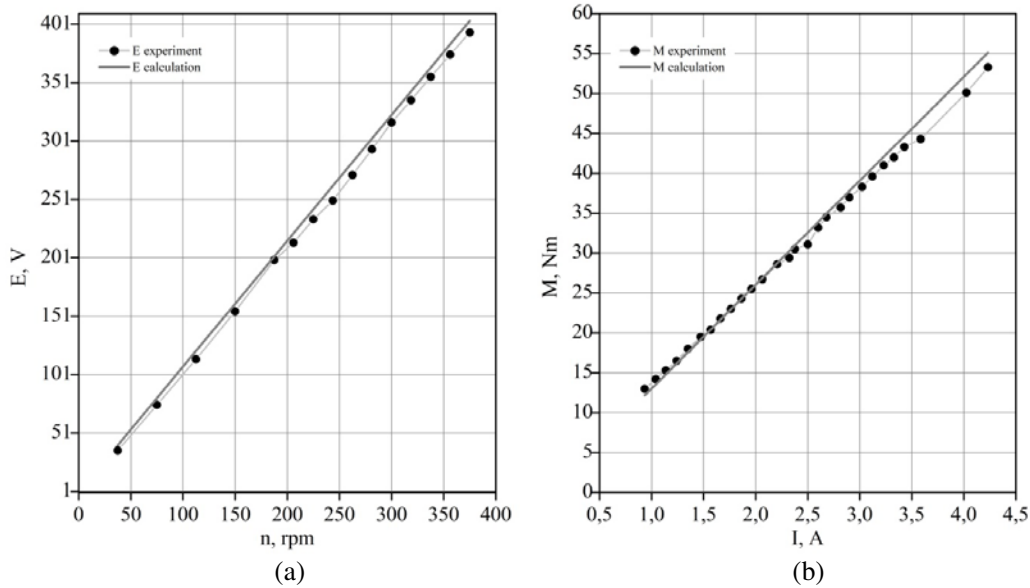


Figure 12. (a) Characteristic of the no-load axial flux electric machine and (b) dependence of the torque on the current in the winding.

Below is a comparison of simulation results with experiment. Figure 12 shows the characteristic of the no-load electric machine, as well as the dependence of the torque on the current in the winding. The dots mark the values obtained experimentally on the stand, and solid lines show the values obtained by simulation.

To determine the back EMF of an electric machine, the magnetic flux through the coils was computed after which the value of the EMF was determined using numerical differentiation. Figure 12(a) shows the rms voltage of the electrical machine between phases.

Figure 13 shows the EMF of an electric machine at the speed of 180 rpm obtained using a 4-channel digital oscilloscope. Figure 14 shows the dependence of the EMF on time obtained by simulation.

The shape of the EMF curve is explained by the fact that there are rather large gaps between the permanent magnets on the rotor (Figure 7). This magnet geometry is not optimal. However, in the future, it is planned to place interpole magnets in the gaps between the magnets to improve the characteristics of the electric machine.

Using a Gauss meter, the magnetic field was measured in the non-magnetic gap of the axial flux electric machine (Figure 15).

Figure 16 shows field plots plotted for points located at the center of the gap above the center line of the magnet in the radial direction. Here, the solid line is the magnetic flux density obtained by simulation, and the dots show the values of the magnetic flux density measured by the device.

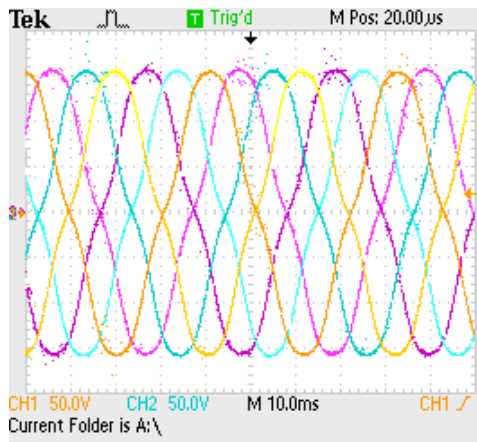


Figure 13. Oscillograms of the generator EMF.

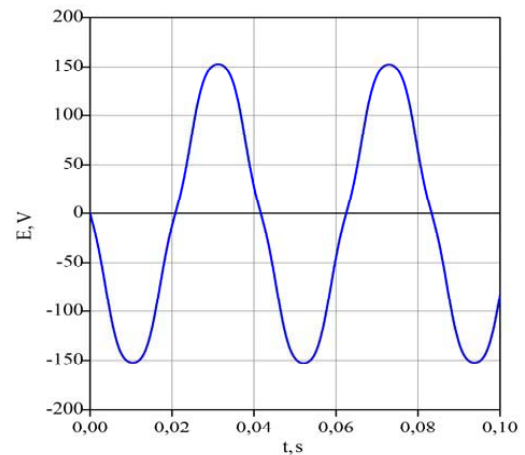


Figure 14. EMF on time (simulation).

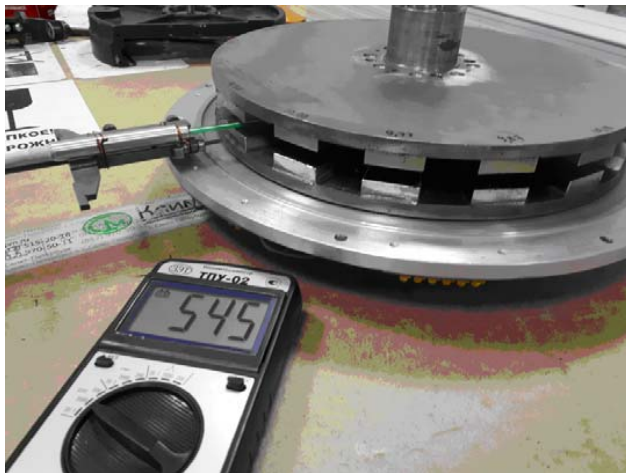


Figure 15. Measurement of the magnetic field in the non-magnetic gap of an electric machine.

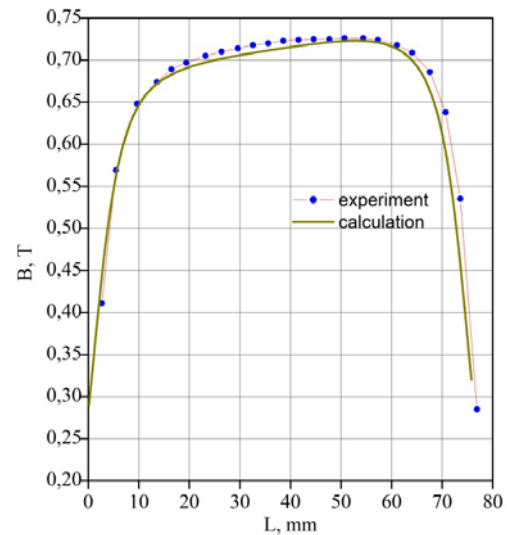


Figure 16. Distribution of the magnetic field in the machine gap.

It can be seen from the data presented that the proposed numerical model in Eq. (18) quite adequately describes the distribution of the three-dimensional magnetic field created by the magnetic system of the axial flux machine. Integral characteristics such as the root mean square value RMS of the EMF or the average value of the torque (Figure 12) differ from the experimentally measured values by no more than 3.1%.

We also note that the developed numerical model in Eq. (18) gives an absolute match of the results to the well-known conventional method, which is based on solving the boundary integral equation with respect to a single layer of fictitious magnetic charges. Simulation by the method of a single layer of fictitious magnetic charges was carried out for the same electric machine in [20].

Note that this article should not be taken as a study of electric machines. The main goal of the article is to develop a numerical simulation method using an improved model of a double layer of fictitious magnetic charges. The main problem of this subsection is to compare the simulation results with the measurement results at a real technical object, and in this case, this object is an axial flux machine.

Using the mathematical model developed in this article, a new structure of an axial flux machine

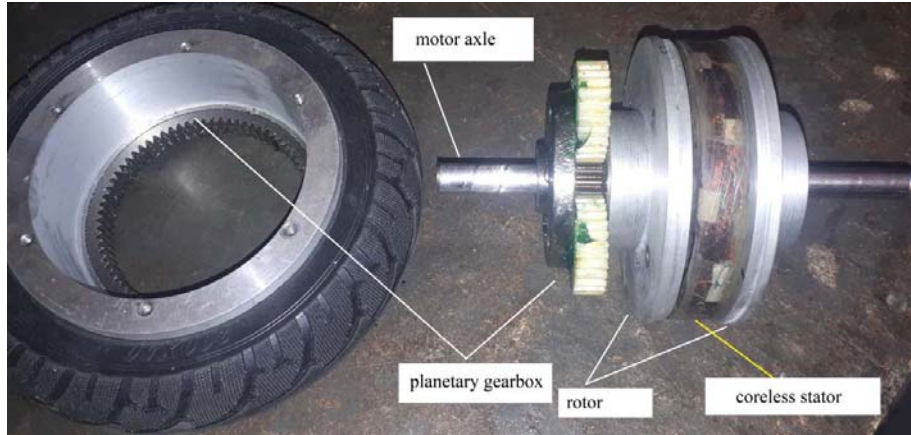


Figure 17. Vehicle in-wheel motor with the coreless axial flux electric machine.

was designed. A feature of this structure is a nonuniform non-magnetic gap along the radius. This solution made it possible to ensure the densest filling of the stator with copper, and also significantly (by more than 10%) increase the magnetic flux in the gap of the electric machine. The proposed design of an axial flux machine can be used in electric transport as a traction motor built into a vehicle wheel (Figure 17).

Table 1 shows the main parameters of the manufactured coreless axial flux electric machine for an electric scooter in-wheel motor.

Table 1. Parameters of the new coreless axial flux electric machine for an in-wheel motor.

Parameter	Unit	Value
Reduction ratio	—	5
Rated/Peak torque input of the gearbox	$N \times m$	1.2/2.5
Rated/Peak torque output of the gearbox	$N \times m$	6/12.5
Rated rotational speed input of the gearbox	rpm	3150
Rated rotational speed output of the gearbox	rpm	630
Outer diameter of coreless stator,	mm	106
Mechanical air gap	mm	0.6
Number of poles	—	8
Voltage DC	V	9
Current DC	A	47
Motor power	W	425
Magnet type	—	NdFeB, N50
Weight of permanent magnets	kg	0.425
Weight of magnetic system	kg	2

It can be seen from the table that the rotor speed of the new electric machine is over 3000 rpm. In general, the magnetic system was designed for a speed of 10000 rpm. However, such a speed requires the use of a planetary gearbox with an increased gear ratio (8 or 10) so that the gearbox output speed does not exceed 1000 rpm. The prototype shown in Figure 17 used a gearbox with a gear ratio of 5. In the future, it is planned to design and manufacture a gearbox with a gear ratio at least 10.

The new coreless axial flux electric machine is designed to operate in fairly high-speed modes. Since the winding of coreless axial flux electric machine is completely penetrated by the time-varying magnetic

flux of the rotating rotor, eddy currents are induced in the winding wire. Since the rotor speed of this machine is quite high, it is necessary to estimate the eddy current losses in the conductors of the stator coils.

This will be the subject of our further research.

5. CONCLUSION

The secondary sources method for analysis of a stationary magnetic field based on the use of a double layer of fictitious magnetic charges is more preferable in comparison with other types of boundary secondary sources. However, the conventional implementation of the method, which is based on numerical solution of the boundary integral Equation (1), requires calculating the scalar magnetic potential, which is usually a multi-valued function.

It is shown, for the first time, that when solving the integral Equation (1) numerically by introduction of a piecewise constant approximation of double layer density, the interface conditions of the field are not fulfilled at any point of the interface. However, the interface conditions are fulfilled integrally.

Based on the application of integral relations following from the Ampere's Circuital Law, which is written with respect to the vector of the magnetic field strength and then with respect to the vector of the magnetic flux density, a new system of linear equations is obtained with respect to the coefficients of piecewise constant approximation of double layer density.

The total current law is written with respect to contours that are infinitely close to the interface. The article discusses the most rational way to define these contours. A method of calculating the integrals included in the coefficients of the obtained system of equations is proposed. This method is developed for a fairly general case because the triangulation of a surface of ferromagnetic samples is considered.

The resulting system of Equation (18) does not contain the scalar magnetic potential of free sources and, therefore, can be directly applied to the analysis of magnetic field in any multiply connected domains without introducing impenetrable partitions or solving an additional boundary value problem for finding the scalar magnetic potential. The new method is as economical as the classical double layer method of fictitious magnetic charges which is based on the solution of integral Equation (1).

The resulting system of Equation (18) is not directly derived from the boundary integral Equation (1). The kernel of the integral included in Eq. (18) differs from the kernel of the integral Equation (1). The mathematical derivation of the system of Equation (18) differs from the derivation of the boundary integral Equation (1). From this, we conclude that the method proposed in the article is an independent method, which is alternative to the classical method of integral equations.

On the basis of the developed method, the simulation of the magnetic field generated by the axial flux electric machine was carried out. It is shown that the simulation results are significantly consistent with experimental data.

A new promising design of an axial flux machine with an increased stator fill factor is proposed. In further research, the new method of a double layer of fictitious magnetic charges developed in the article will allow performing an accurate estimation of eddy current losses in the stator winding of a new electric machine. This will optimize the design of the new electric machine in terms of minimizing the total copper losses (Joule losses and eddy current losses).

ACKNOWLEDGMENT

The reported study was funded by RFBR, project number 20-08-00962.

REFERENCES

1. Muzychuk, Y., "On Green's function in boundary elements method for some infinite triangular system of elliptic equations," *XXth IEEE International Seminar/Workshop on Direct and Inverse Problems of Electromagnetic and Acoustic Wave Theory (DIPED)*, 147–150, Lviv, Ukraine, Sept. 2015.

2. Shi, Y. and Z. Wang, "Calculating for surface electric field of converter valve shield system with fast multipole curved boundary element method," *The Journal of Engineering*, Vol. 2019, No. 16, 1575–1579, 2019.
3. Adelman, R., N. A. Gumerov, and R. Duraiswami, "FMM/GPU-accelerated boundary element method for computational magnetics and electrostatics," *IEEE Transactions on Magnetism*, Vol. 53, No. 12, 1–11, 2017.
4. Buchau, A., W. Hafla, W. M. Rucker, "Accuracy investigations of boundary element methods for the solution of Laplace equations," *IEEE Transactions on Magnetism*, Vol. 43, No. 4, 1225–1228, 2007.
5. Hafla, W., A. Buchau, F. Groh, W. M. Rucker, "Efficient integral equation method for the solution of 3-D magnetostatic problems," *IEEE Transactions on Magnetism*, Vol. 41, No. 5, 1408–1411, 2005.
6. Takahashi, Y., C. Matsumoto, and S. Wakao, "Large-scale and fast nonlinear magnetostatic field analysis by magnetic moment method with adoptive cross approximation," *IEEE Transactions on Magnetism*, Vol. 43, No. 4, 1277–1280, 2007.
7. Kim, D. H., I. H. Park, M. C. Park, and H. B. Lee, "3-D magnetostatic field calculation by a single layer boundary integral equation method using a difference field concept," *IEEE Transactions on Magnetism*, Vol. 36, No. 5, 3134–3136, 2000.
8. Andjelić, Z. and K. Ishibashi, "Double-layer BEM for generic electrostatics," *2016 IEEE Conference on Electromagnetic Field Computation (CEFC)*, 1–1, Miami, FL, USA, Nov. 2016.
9. Andjelić, Z., K. Ishibashi, and P. D. Barba, "Novel double-layer boundary element method for electrostatic analysis," *IEEE Transaction on Dielectrics and Electrical Insulation*, Vol. 25, No. 6, 2198–2205, 2018.
10. Ishibashi, K., T. Yoshioka, S. Wakao, Y. Takahashi, Z. Andjelic and K. Fujiwara, "Improvement of unified boundary integral equation method in magnetostatic shielding analysis," *IEEE Transactions on Magnetism*, Vol. 50, No. 2, 1–4, 2014.
11. Ishibashi, K., Z. Andjelic, Y. Takahashi, T. Takamatsu, T. Fukuzumi, S. Wakao, et al., "Magnetic field evaluation at vertex by boundary integral equation derived from scalar potential of double layer charge," *IEEE Transactions on Magnetism*, Vol. 48, No. 2, 459–462, 2012.
12. Ishibashi, K. and Z. Andjelic, "Generalized magnetostatic analysis by boundary integral equation derived from scalar potential," *IEEE Transactions on Magnetism*, Vol. 49, No. 5, 1533–1536, 2013.
13. Ishibashi, K., Z. Andjelic, Y. Takahashi, Y. Tawada, T. Yoshioka, S. Wakao, et al., "Nonlinear magnetostatic analysis by unified BIE utilizing potential gap due to loop currents," *IEEE Transactions on Magnetism*, Vol. 49, No. 5, 1573–1576, 2013.
14. Telegin, A. P. and N. I. Klevets, "Calculation of an axisymmetric current coil field with the bounding contour integration method," *Jornal of Magnetism and Magnetic Materials*, Vol. 277, 257–262, 2004.
15. Filippov, D. M. and A. A. Shuysky, "Improving efficiency of the secondary sources method for modeling of the three-dimensional electromagnetic field," *Progress In Electromagnetics Research M*, Vol. 78, 19–27, 2019.
16. Filippov, D. M.; G. P. Kozik, A. A. Shuysky, A. N. Kazak, and D. V. Samokhvalov, "A new algorithm for numerical simulation of the stationary magnetic field of magnetic systems based on the double layer concept," *2020 IEEE Conference of Russian Young Researchers in Electrical and Electronic Engineering (EIConRus)*, 647–652, St. Petersburg and Moscow, Russia, Jan. 2020.
17. Neethu, S., S. P. Nikam, A. K. Wankhede, S. Pal, and B. G. Fernandes, "High speed coreless axial flux permanent magnet motor with printed circuit board winding," *IEEE Industry Applications Society Annual Meeting*, 1–8, Cincinnati, OH, USA, Oct. 2017.
18. Aydin, M. and M. Gulec, "A new coreless axial flux interior permanent magnet synchronous motor with sinusoidal rotor segments," *IEEE Transactions on Magnetism*, Vol. 52, No. 7, 1–4, 2016.
19. Price, G. P., T. D. Batzel, M. Comanescu, and B. A. Muller, "Design and testing of a permanent magnet axial flux wind power generator," *Proceeding of the 2008 IAJC-IJME International Conference*, Music City Sheraton, Nashville, TN, USA, Nov. 2008.

20. Filippov, D. M., A. A. Shuyskyy, and A. N. Kazak, "Numerical and experimental analysis of an axial flux electric machine," *2020 International Conference on Industrial Engineering, Applications and Manufacturing (ICIEAM)*, 1–6, Sochi, Russia, 2020.